Aarhus University

Master's Thesis

Beta-decay of 8Li: beta-alpha correlations and final state distribution

Author:
Anders Holst Rasmussen
201606907

Supervisor:
Hans O. U. Fynbo

June 10, 2021

Contents

1 Introduction

1.1 Motivation

When Henri Becquerel first discovered radioactivity in the 1890's, a new branch of atomic physics was born, namely nuclear physics, which is the study of the atomic nuclei, their constituents and interactions. Over the years it has evolved quickly, first by the discovery of three different types of radiation by Curie and Rutherford, to the discovery of different nucleons, that the nucleus itself is made of.

The technological advancements has made the study even more precise over the years, as the development of radioactive beams allow for the creation of specific short lived isotopes. This technique is known as Isotope Separation On-Line (ISOL), which was first developed in 1951 for the Copenhagen Cyclotron. Now the technology is available in many parts of the world, such as the IGISOL facility at the University of Jyväskylä in Finland [1]. Another important advancement is the development of very precise detectors, such as the Double Sided Silicon Detector (DSSD), which allows for a very high energy and spacial resolution, which can give a detailed analysis of both coincidence and kinematics.

This brings us onto the current experiment that I have analyzed in this thesis. At the IGISOL facility, the experiment I257 was carried out in august 2020. The objective of the experiment was to measure β-decays from ^{8}Li and ^{12}B, however, this thesis will only govern the ^{8}Li decay.
In precious studies, it has been shown that angle between the β-particle and the α-particles are very close to isotropic [2]. The study of the β-α correlation in ^{8}Li will therefore serve as a good indicator for the β-α correlation in

^{12}B, as the same setup will be used for both experiments.
A former student has previously made an in depth analysis of the mirror nucleus ^{8}B, which can be used to compare the excitation energy of ^{8}Be [3].

1.2 Nuclear decays

Lithium normally occurs stable as ^{6}Li and ^{7}Li, with the latter being the more abundant with 92.5% of all atoms. The longest living radioactive lithium isotope is ^{8}Li, with a half-life of 839 ms [4]. When ^{8}Li decays, it will do so by a β-decay, immediately followed by the α-α breakup of an intermediate exited state in ^{8}Be, which has a half life of 1×10^{-16} s. ^{8}Be is a constituent in the triple-alpha process in stellar astrophysics, and creates a bottleneck for the creation of heavier elements, because of its very short lifespan.

1.2.1 β-decay

Most light unstable nuclei will decay by either proton/neutron emission, or by a β-decay. Isotopes that lie close to the valley of stability will not decay by proton/neutron emission, but from a β-decay.
A β-decay is a weak interaction, which allows a quark in a proton or neutron to change flavor, by emitting a W boson. This leads to the creation of either an electron/antineutrino pair or a positron/neutrino pair:

$$\beta^+ : \quad p \rightarrow n + e^+ + \nu_e \tag{1.1}$$

$$\beta^- : \quad n \rightarrow p + e^- + \bar{\nu}_e. \tag{1.2}$$

Nuclei below the valley of stability will decay by β^-, while nuclei above decays by β^+.
The energy of these decays are given by their Q-values, neglecting the very small neutrino mass and the binding energy of the electrons gives:

$$Q_{\beta^+} = \left[m(^{A}_{Z}\mathrm{X}) - m(^{A}_{Z-1}\mathrm{X}')\right] c^2 \tag{1.3}$$

$$Q_{\beta^-} = \left[m(^{A}_{Z}\mathrm{X}) - m(^{A}_{Z+1}\mathrm{X}') - 2m_e\right] c^2, \tag{1.4}$$

where m is the mass of an atom with Z protons and A nucleons. The Q-values indicates the mass difference between the initial and final product., which can be either excitation energy or kinetic energy.
Not all β-decays are allowed. If the spin is unchanged, it is a Fermi transition, and if it changes it is a Gamow-Teller transition. An allowed decay is a transition with the change in orbital angular moment $\Delta L = 0$, and forbidden transitions have $\Delta L > 0$.
The nuclear part of the β-decay operator for an allowed decay is:

$$\mathcal{O}(\beta^{\pm}) = g_V \sum_{A}^{j=1} \tau_{\mp}(j) + g_A \sum_{A}^{j=1} \sigma(j)\tau_{\mp}(j), \tag{1.5}$$

where g_V is the weak vector coupling constant, $\tau_{\mp}$ is the isospin step operator, g_A is the weak axial coupling constant and σ is the Pauli spin matrices. The first term corresponds to the Fermi operator, and the second term to the Gamow-Teller operator. This raises some selection rules, that dictate that for a Fermi decay, spin, isospin and parity must not be changed, and for a Gamow-Teller transitions, $\Delta J = 0, \pm 1$, $\Delta T = 0, \pm 1$, and $\Delta \pi = 0$.
The selection rules then enforces that not every energy level is populated in ^{8}Be.

The ground state of ^{8}Li has spin, parity and isospin of $2^+; 1$, and a mass of $16.005\,\mathrm{MeV/c^2}$ more than the ground state of ^{8}Be, so it will only be able to populate states with lower energy than $16.005\,\mathrm{MeV}$, and states where the transition rules applies.
Looking at the states in ^{8}Be, there are only 3 states below the threshold of $16.005\,\mathrm{MeV}$, that is the ground state, first and second excited state. The ground state is a $0^+; 0$ state, with $\Delta J = 2$, which is forbidden given the selection rules.
The first excited state is a broad state at $3.03\,\mathrm{MeV}$ and $2^+; 0$, which gives $\Delta J = 0, \Delta \pi = 0$ and $\Delta T = 1$. This transition is valid within the selection rules, and is in fact the only state that will be populated in the decay.
The second excited state at $11.35\,\mathrm{MeV}$ is a $4^+; 0$, where $\Delta J = 2$, so the state

will not be populated either. The energy levels and properties can be seen on fig. 1.1.

1.2.2 α-decay

α-decay is another type of radioactive decay, where the nucleus emits an α-particle, and thereby decays into a different nucleus with the atomic number reduced by two. It has a Q-value of:

$$Q_\alpha = \left[m(^{A}_{Z}\mathrm{X}) - m(^{A-4}_{Z-2}\mathrm{X}') - m_\alpha\right] c^2. \tag{1.6}$$

Usually it is only elements heavier than nickel that can decay via this process, as the binding energy per nucleon decreases, and therefore becomes unstable towards spontaneous fission type processes. One of the only exceptions to this, is ^{8}Be, which is one of the only light nuclei that decays by α-decay.

1.2.3 Production of ^{8}Li

The production of ^{8}Li is rather crucial to the existence of the experiment, which is why the experiment had to be conducted at IGISOL in Jyväskylä, Finland. This facility is specialized in creating near stable isotopes of many elements and make them into a beam.
In simple steps, the stable ^{7}Li is hit by a deuteron, where the neutron will stick to the the nucleus of ^{7}Li, and create ionized ^{8}Li. When it becomes ionized, it can be accelerated into a beam and shot at the target. The target is a thin carbon foil, where the ionized ^{8}Li will be stopped and lie. The target will transfer an electron to ^{8}Li, making it not ionized, and we are left with pure ^{8}Li just where we want it.

1.3 Structure of ^{8}Be

Figure 1.1 shows the excitation spectrum for ^{8}Be, with values from [4]. The spin, parity and isospin are written as $J^\pi;T$ for each level. 4 different states has been shown for ^{8}Be, where only the first excited state is the broad state

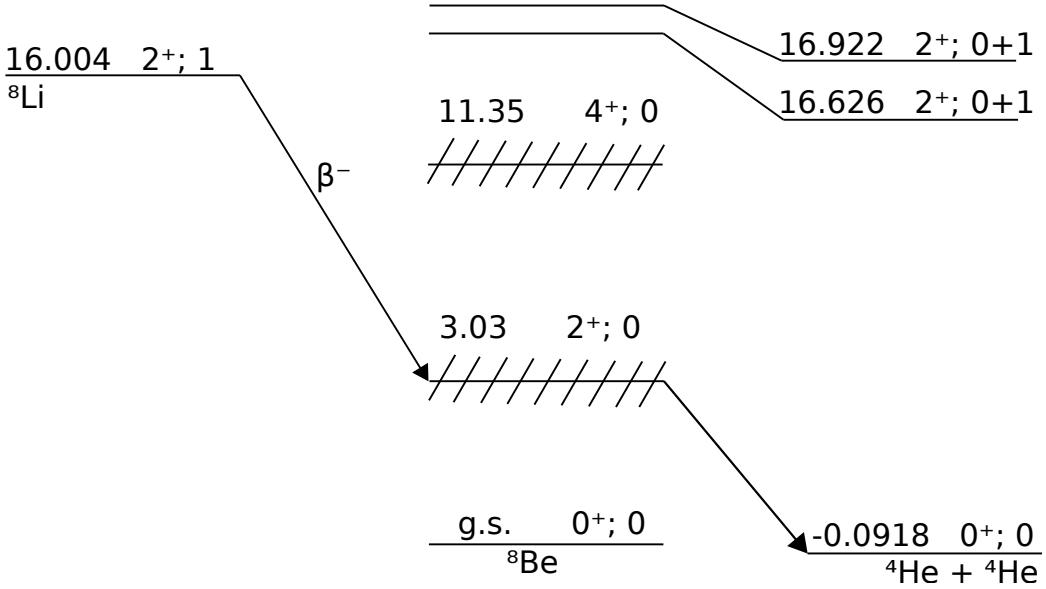

Figure 1.1: The decay scheme of ^{8}Li, and some notable excitation energies of ^{8}Be. Each level is labeled with the energy above the ^{8}Be ground state in MeV. Spin parity and isospin is noted as $J^\pi; T$. All information is from [4].

at 3.03 MeV. This state has conservation of spin and parity from ^{8}Li and is the only state that is allowed for the decay of ^{8}Li. Situated above is the broad state at 11.35 MeV, which does not conserve spin. Above that is a 16.626 MeV state, which conserves spin, parity and isospin, but lies energetically above ^{8}Li, so we would not expect that to shown in the data. It is still a quite relevant state, as the mirror nucleus ^{8}B $(2^+; 1)$ lies just above the energy at 17.979 MeV, and then has enough energy to populate this state, even though it is not very likely. Previous experiments made by the Aarhus subatomic group has examined the decay, and found only 5 counts populating this excitation level. But that should not show up when looking at the decay of ^{8}Li.

2 Experimental Methods

The main goal of the experiment was to determine the β-α angular correlation. The experiment was done at the IGISOL facility, at the University of Jyväskylä, where beams of all elements can be produced. The experiment took place in august 2020, delayed by the ongoing corona pandemic. This chapter will be concerning the experimental setup, a discussion of the detectors and an overview of the software used to extract and analyze the data.

2.1 Detector setup

The setup is designed mainly for the decay of 12B measured in the same experiment. In that decay three-alpha particles are emitted in less than 1% of the decays and the setup should therefore have a high efficiency and be able to measure α-particles in an environment with many beta-particles.

2.2 Experimental setup

The setup is able to measure $\beta - \alpha$ angular correlations in the β-delayed particle decay of ^{8}Li. When measuring multiple particles, the setup is highly dependent on the coverage of the solid angle. Therefore the setup is designed to have a large solid angle coverage, with high α-particle resolution, while still being able to measure β-particles.
This is has been achieved by creating a cube of six double sided silicon detectors (DSSD), all backed by a unsegmented silicon detectors (PAD). To gain the largest solid angle, the detectors where placed as close to one another as possible. A 3D printed case was designed to hold the detectors in place, and achieved a solid angle coverage of 51% for the DSSD's, which can be seen

on fig. 2.1. An illustration of the setup, together with the different detectors' thickness can be seen on fig. 2.2. Even though the setup was designed to hold 12 detectors in total, there where only 11 detectors in the actual experiment. The PAD behind Det1 was defect, and was therefore removed.

Detector	Thickness [μm]	PAD	Thickness[μm]
Det1	67	n/a	n/a
Det2	1002	P2	1036
Det3	65	P3	1497
Det4	60	P4	1490
DetU	60	PU	1498
DetD	1043	PD	1038

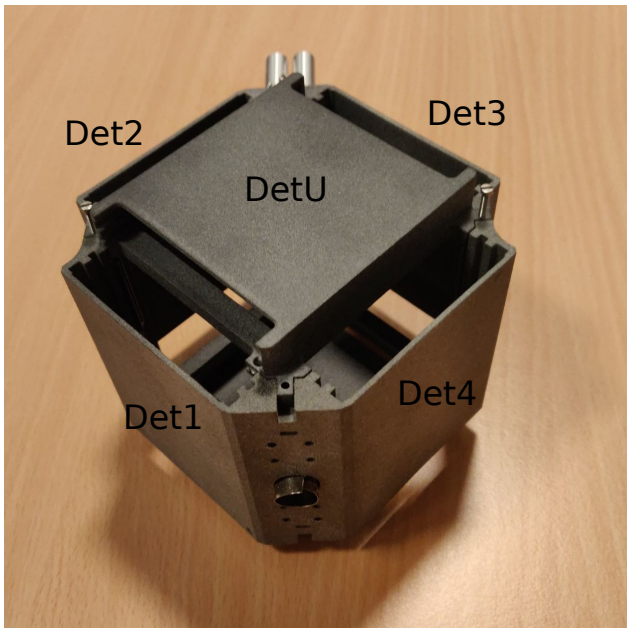

Figure 2.1: A picture of the 3D printed cube used to hold all detectors in place. The placement of the detectors have been shown, with exception of DetD, which was at the bottom of the cube. The beam enters the metal ring between Det1 and Det4

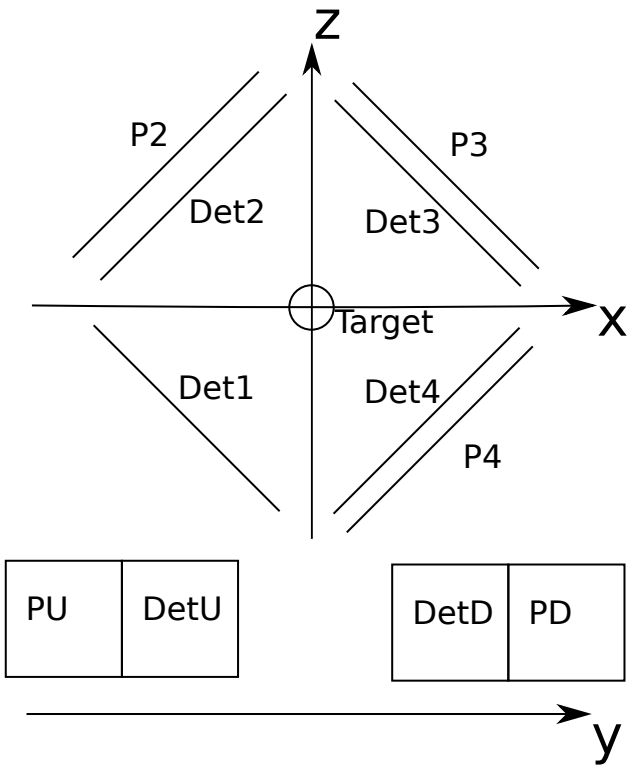

Figure 2.2: An illustration of the setup. Det1-Det4 are placed around the target, facing the target which is located at the center of the coordinate system. DetU is above the target, and DetD is below the target. Behind each detector is a PAD, with the exception of Det1, who's PAD was defect. The beam is parallel to the z-axis, entering the setup from the negative z-direction.

2.3 The detectors

As mentioned above, there where two types of detectors present in the setup. The first type is the Double sided silicon detector. As the name suggests, it consists of two sides, a front layer and a back layer. Each layer consists of 16 strips, that are placed in rows next to each other. The two layers are then arranged so each side are mutually orthogonal, which effectively makes pixels where each strip intersects a strip on the other side. An illustration of the detector can be seen on fig. 2.3.

The strips on the front side are p-doped, while the back side are n-doped.

When a charged particle hits the detector, it will ionize the atoms in the semi-conductor, and produce a electron-hole pair. The number of electron-hole pairs is proportional to the energy of the charged particle. The bias voltage on the detector collects the electrons and holes on opposite sites of the strip, where the charge is collected on aluminum contacts and a signal is measured. Energy is not deposited in these contacts, and therefore they constitute to a so called dead layer.
The detectors are square 5×5 cm and with their 16×16 strips, they have an effective gird of 256 pixels of 9 mm. 4 of the 6 detectors have a thickness of 60 μm and a 100 nm dead layer. These detectors are the ones called Det1, Det3, Det4 and DetU in the setup seen on fig. 2.2. The other 2 detectors (Det2 and DetD) where both 1000 μm.

The other type of detector is the PAD. They are different from the DSSD's, in that they do not have sides, and no strips. Therefore they do not contain a grid, the same way the DSSD's do, and will not provide any information as to where a particle has hit. But they are included in the setup to detect excess energy of particles not stopped by the DSSD. This makes them good at detecting β-particles, as they will not be stopped by a DSSD.
An α-particle will deposit all of its energy into the first DSSD it encounters, and be effectively stopped completely by it, and a β-particle will deposit almost no energy in a thin DSSD, and travel through it, ending up depositing some energy in the PAD.
Therefore one can roughly distinguish the α-particles from the β-particles, by observing whether a particle has hit the DSSD and the PAD.

Since there are also two thick DSSD's in the setup, one can also get some information from a β-particle from these thicker detectors, as it will deposit more energy in these detectors.

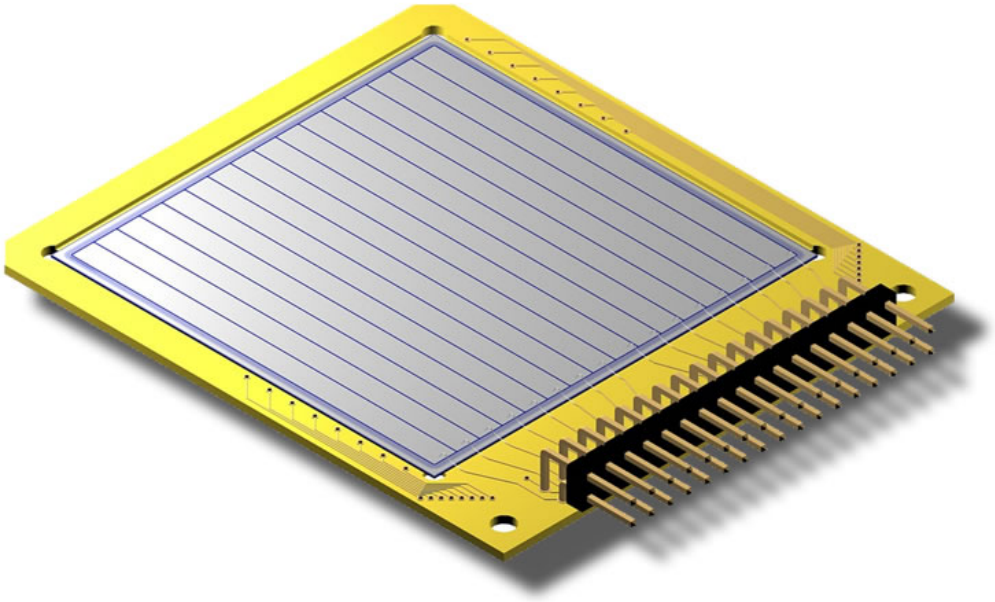

Figure 2.3: An illustration of the DSSD type used in this experiment. The detector has 16 p-doped strips, and 16 n-doped strips perpendicular to these. This gives 256 pixels for the detector. Image courtesy of Micron Semiconductor Ltd

2.4 AUSAlib and ROOT

ROOT [5] is an object oriented C++ framework that is designed primarily for data analysis in high-energy and nuclear physics. It was created at CERN in 1995, and has since grown and become the dominant analysis software at both CERN and many other nuclear and particle physics laboratories. ROOT was designed to handle large amounts of data with high computing efficiency.

ROOT makes an intelligent data structure by creating a "Tree" with the class `TTree`. This tree will then have "branches" which corresponds to some variable of the given detection event, such as the energy of the front strip or identity of the detector. This `TTree` then allows for reading of an individual

branch, while ROOT takes care of the memory management. One can also store a `TTree` to the disk in the form a .root file.

ASUALib [6] is a tool that build on top of ROOT. It was created by the subatomic group at Aarhus University. Before this tool was created, everyone in the group had to more or less create their own tools to get data from the detectors into a useful data structure. This meant that a lot of time was wasted just trying to access data from experiments. AUSAlib was therefore created, so the basic tasks of data extraction was automated.
AUSAlib has a lot of functionalities, but the two main tools that was used to extract data was the *Sorter* and *Calibrator*.

2.4.1 Unpacker

The `Unpacker` converts raw data from the detectors into a ROOT TTree. This is done by using the unpacking program `ucesb` [7]. This will setup the branch structure of the data. Some of these branches are `FT` and `BT`, which is a vector of the `TDC` (time) values for each event, for the front and backside of the detector. They are vectors because they contain information for each particle hits in a given time slot, for which there can be multiple. There are also the branches `FE` and `BE`, which is the `ADC` (energy) associated with the events.

2.4.2 Calibrator

Since the detectors work, by measuring an electrical charge that comes from the charged particle, the detectors needs to translate a specific charge to energy deposited.
To do that, we use the `Calibrator`-tool, which is designed to convert a channel number into an actual energy. Assuming that the channel numbers are linearly related to the energies, a known radioactive source can be measured, and the expected spectrum can be compared to the measured. This is done for each strip in each detector.

The `Calibrator` starts by running a peak-finding algorithm over some calibration data, to roughly identify the locations of the peaks, followed by a multi-Gaussian fit to find the most precise peak location. The positions of the peaks can then be compared to the expected energies, giving an associated energy to a given channel.

As mentioned earlier, all of the detectors have a small aluminum dead layer. All particles that pass through this layer will loses some amount of energy depending on the stopping power of the material and the effective thickness of the dead layer Δx_{eff}, which furthermore depends on the angle of incidence, θ. The relationship between the effective thickness and the actual thickness is described as $\Delta x_{eff} = \Delta x / \cos(\theta)$. This gives the measured energy as

$$E' = E - \frac{dE}{dx}\frac{\Delta x}{\cos(\theta)},$$

where E is the original energy of the particle, dE/dx is the stopping power of the material and Δx is the thickness of the dead layer. The stopping power is calculated from SRIM [8]

These calculations are all handled by the `Calibrator`. As input it takes an unpacked measurement of a source, a file specifying the locations of the expected peaks and a file specifying the spacial locations of the detectors. From this it calculates the energy loss, and creates a linear relationship between channel numbers and energies. This is then written to the disk as a seperate calibration file, which can be parsed to other modules.
It is important to note that the Calibrator does not modify any data. Therefore the energy loss is unaccounted for. Instead it corrects the expected energy spectrum, which means that the resulting calibration is still valid. The energy loss correction is therefore still needed in the analysis, as the effect is unaccounted for in measurements.

2.4.3 Sorter

The sorter is used after a successful calibration. It generates a ROOT file based on the unpacked data, and applies the calibration. It is also responsible for matching and combining events from the front-side to the back-side of the detector. If there where one hit in the front side and one in the back, the mathcing is fairly trivial. If there however where multiple hits in both front and back, the `Sorter` will run a matching algorithm, which pairs the hits with the lowest energy differences.

When the events have been matched, the hits on the individual sides of each detector are merged into a single event. Therefore each event can now be considered a multiple of particle hits. This makes it possible to to associate physical properties with each particle, such as direction and energy. There has still not been done any filtering of the data, which is what we will discuss in chapter 3.

3 Data Reduction

3.1 Calibration

To actually calibrate the detectors, we use an α-source with a known spectrum. The source is placed in the target position, and each detector is in turn placed in front of the source. The radioactive source used to calibrate this setup contained ^{148}Gd, ^{239}Pu and ^{244}Cm. Each isotope has a prominent main peak, and several sub peaks. The proprieties of which is listed in table 3.1.

Isotope	E_α $[keV]$
^{148}Gd	3182.690
^{239}Pu	5105.5
	5144.3
	5156.59
^{244}Cm	5762.64
	5804.96

Table 3.1: Decay energies for each isotope used in the calibration.

A typical single strip spectrum is shown on fig. 3.1a, where the calibrator has given an estimate of where the peaks are, illustrated by the red triangles. fig. 3.1b shows a closer look at the ^{244}Cm peak, where the red line shows the `Calibrator`-fit over both the main peak and the sub peak.

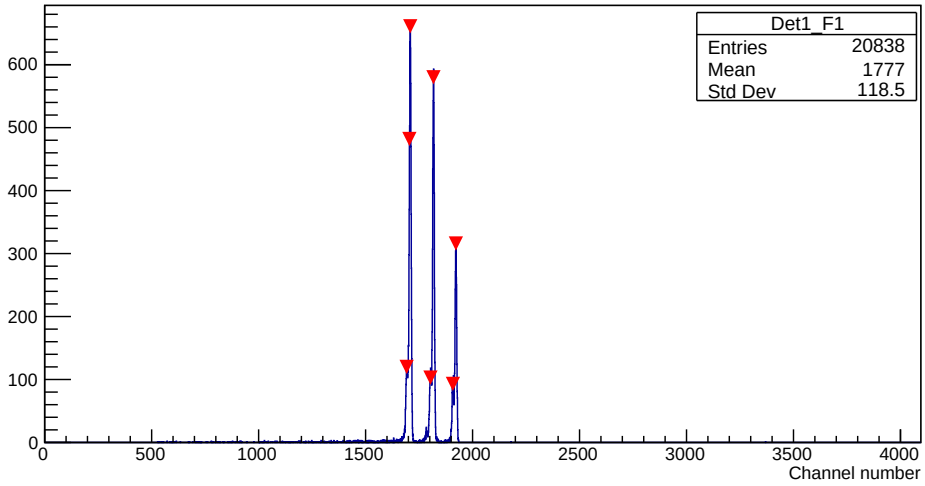

(a) A spectrum of the calibration source, with channel number along the x-axis. The red triangles indicate the positions the `Calibrator` has guessed as the peaks.

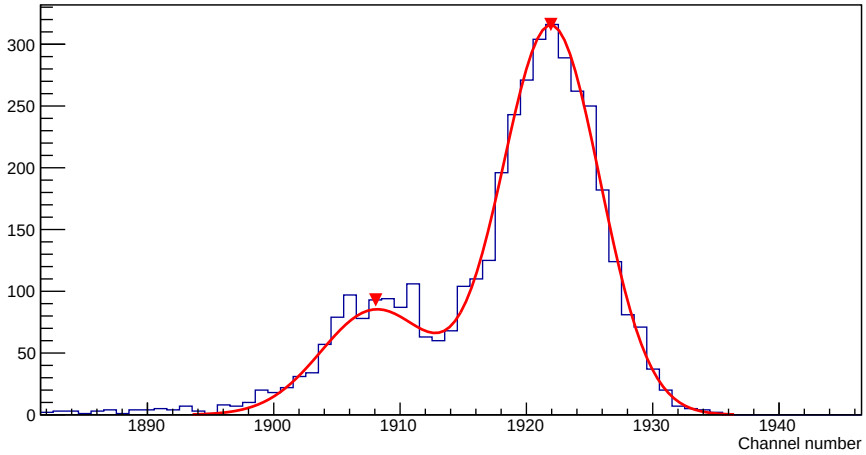

(b) A closer look at the ^{244}Cm peak on the above figure. The red line is a fit performed by the `Calibrator`, and the red triangles indicate the guessed peaks.

Figure 3.1: Calibrations of detector 1

3.2 Identifying the particles

After utilizing the AUSAlib tools, the data is ready to be analyzed. Even though the theory dictates that a decay will consist of two α-particles and one β-particles, it is not realistic to just assume that each detected event will consist only of this configuration of particles.

Therefore we need some cut on what events we will allow through to the analysis. Specifically we are going to impose 3 cuts on the data, a angular cut, a momentum cut and a multiplicity cut.

3.2.1 Identifying a hit

After a hit has been detected, and all the relevant information has been extracted from the hit, we can start to analyze what type of particle has hit the detector.
A important distinction between an α-particle and a β-particle is the different interactions with a detector. An α-particle will be completely stopped by a standard 60 μm detector, while a β-particle will pass through it, depositing only a small amount of energy.
This is the reason for the PAD's behind each DSSD. The idea is that only a β-particle will be detected in the PAD's, so if a hit has some energy in a DSSD *and* the corresponding PAD, it will be classified as a β-particle.

This approach however does not work as well as intended. Often what happens is that the thin DSSD will not pick up any energy deposited, and the hit will therefore not be counted. But not all of the detectors are 60 μm. We have two detectors that are around 1000 μm thick. These detectors are much better at picking up a signal from a β-particle, so one of the criteria for being a β-particle in this setup is to have hit either Det2 or DetD.

These two criteria are however not enough to uniquely determine that a hit was a β-particle. We still have to consider the events where a detector has multiple hits. Since a PAD gives no usable information regarding where a particle has hit, we cannot say which particle was a β-particle and which where an α-particle.
Therefore if the β-particle criteria are true, we mark the particle as a *possible* β. But since it might as well have been a α-particle, we also mark it as such. Every hit that does not uphold to the β-particle criteria are of course marked only as a possible α-particle.

When all the particles have been identified, we impose the first cut to the data. A multiplicity cut that says we need at least two α-particles. If there are less, we discard the event.
When we at least have two distinct particles that can be α-particles, we look at their mutual difference in momentum. The particle pair with the least difference in momentum will be chosen as the only α-particles that can be present in an event. Then we have assured that every other particle we see in the event, is possible β-particle candidates.
When each particle has been identified or discarded, all remaining particle-specific information is stored to the given particle for easy analysis henceforth.

3.3 Angular cut

When ^{8}Be decays, and produces the two α-particles, it will do so under conservation of momentum. The decay in any direction, but the angle θ between them will be close to 180°. Therefore the first cut that we give to the data, is that two of the particles that are α candidates, must have a mutual angle of close to 180°.

On fig. 3.2 a plot of all the the mutual angles are shown. A quick glance will give that most particles will have mutual angle of close to 180°.
By looking at this, we see that most of the angles will lie close to 180°, and now we must decide exactly where to do the cutoff. By taking a sharp cutoff at $\cos(\theta) \geq -0.99$, we will exclude a great deal of good measurements, on the other hand, a too soft cut will not accomplish anything, as too many "wrong" particles will let through the check. By trying different cuts, we have found that $\cos(\theta) \geq -0.95$ is a good cutoff, and this corresponds to 161°.

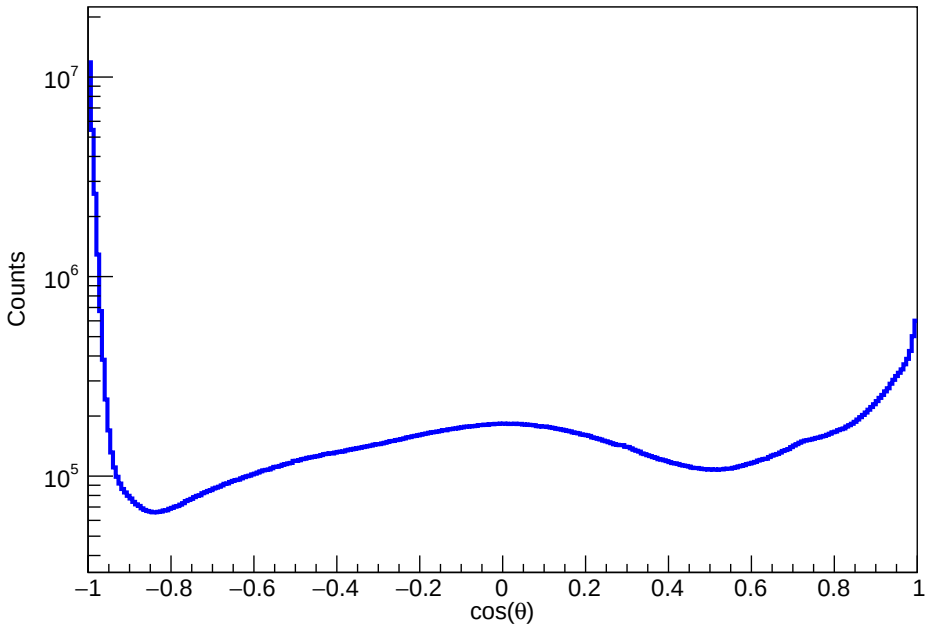

Figure 3.2: A histogram of all the mutual angles between all particles.

3.4 Momentum cut

The second cut we perform on the data is a *total* momentum cut. On fig. 3.3 the total momentum for the two identified α-particles are shown. A prominent peak lies around 13.000 keV/c, and ends around 40.000 keV/c. We impose a cut of maximum 40 MeV/c, as this will include the large amount of pairs lying in the peak, which must be α-αpairs. A α-particle with energy 1500 keV will have a momentum of 105 MeV/c, and a free electron of 3000 keV will have a momentum of 1.7 MeV/c. The majority of particles lies around these energies, and no matter where the β-particle will hit, the total momentum is still much larger than the 40 MeV/c cutoff.

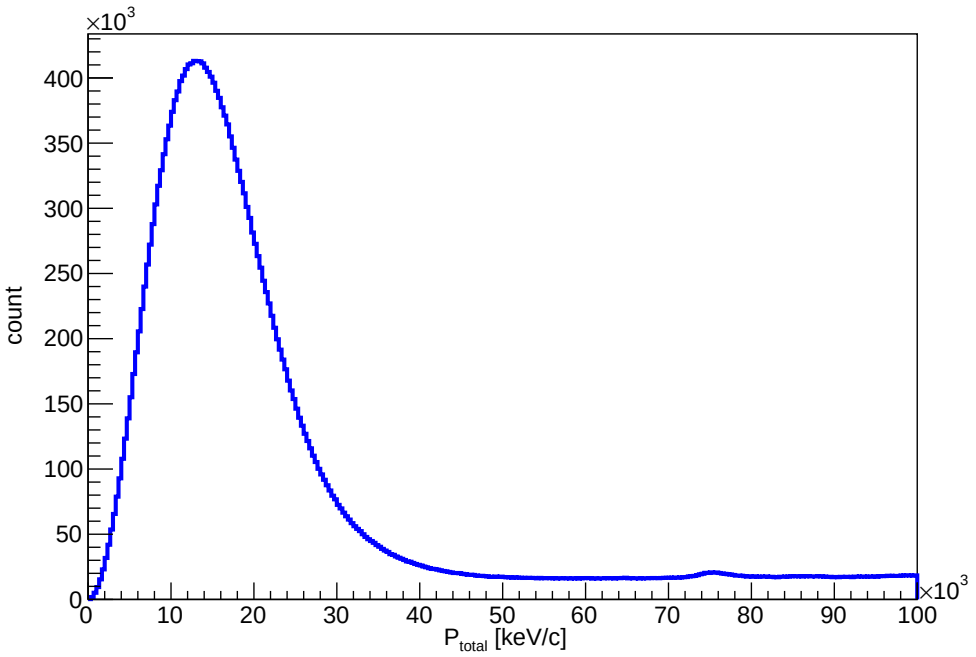

Figure 3.3: The total momentum of the two α-particles.

3.5 Multiplicity cut

The last cut that we want to impose on the data, is a multiplicity cut. This cut is just to ensure that we have the amount of particles that we expect. Therefore a hard criteria is that there must be at least two distinctly identified α-particles.

With regards to the β-particles, we are more loose. Here we say that there must at least be one, but more can occur. This is quite rare, but the we still take that event into account, as the β-particles should have an isotropic distribution, and therefore should not in any case be affected by the other α-particles. On fig. 3.4 we see the multiplicity of β-particles, and in most of the events, we have not detected any β-particles, and when we do, there is a even fewer events with more than one beta. So most of the time, we are in the expected case with two α-particle and one β-particle. add that beta

spreads around in the setup

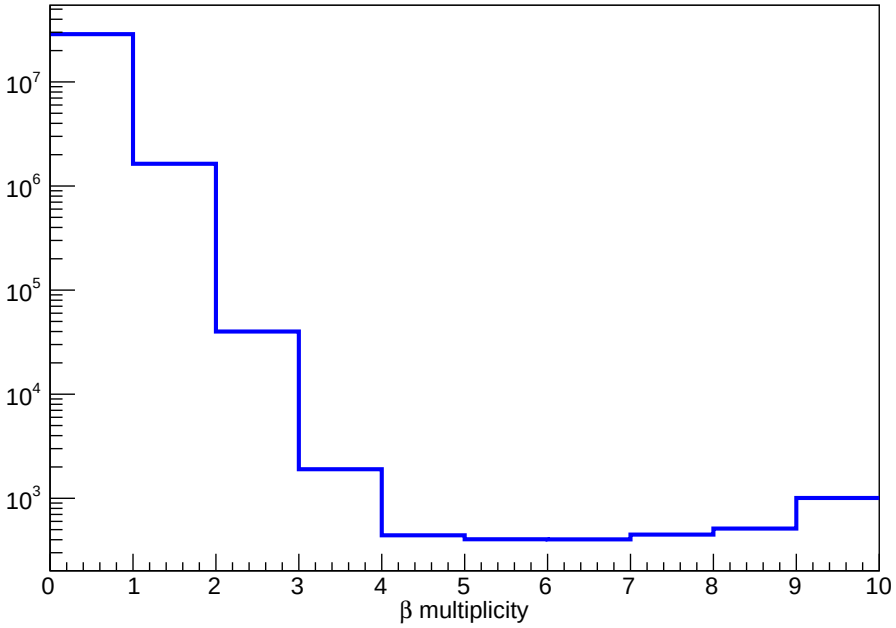

Figure 3.4: The multiplicity of the β-particles.

4 Analysis

4.1 The effects of the cuts

How does the cuts imposed in the previous chapter affect the data then? First we need to look at how the data looks, without any cuts. On fig. 4.1a the energy of the first α-particle ($E_{\alpha 1}$) is plotted against the energy of the second α-particle ($E_{\alpha 2}$). This gives us a nice view of what is considered α-particle pairs. There is a prominent line going diagonally through the graph, where both particles have around the same energy. This line is expected, as the α-particles will have close to equal energy, when decaying from ^{8}Be.
This means that there is a lot of particle pairs that have been identified as α-α, but properbly was α-noise, noise-noise, α-β or β-β pairs.
The lines occurring from $E_{\alpha 2} \approx 400\,\text{keV}$ are a clear example of a α-β pair. In this line, $\alpha 1$ has been identified correctly as a α-particle, which will have energies ranging from 500-6000 keV, whereas the the other particle has a more constant energy, corresponding to the energy a β-particle can deposit in a detector. So by doing no cuts at all, we are left with a lot of cases where we have no real control over what particle type we are dealing with.

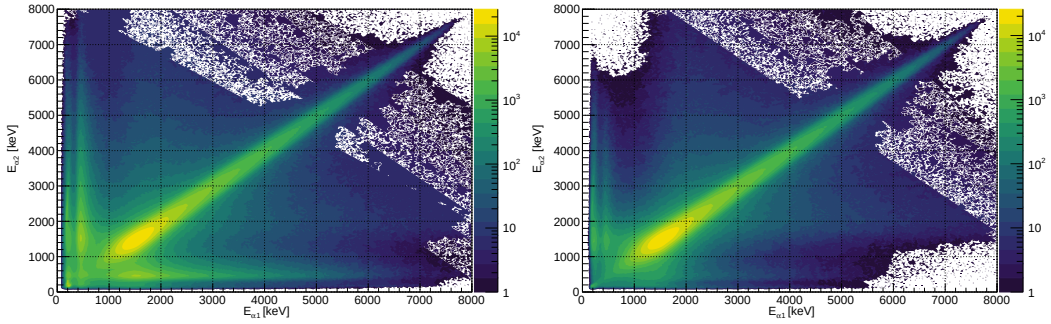

(a) No cuts on the data

(b) An angular cut. The angle between the two partcles must be greater than 160°.

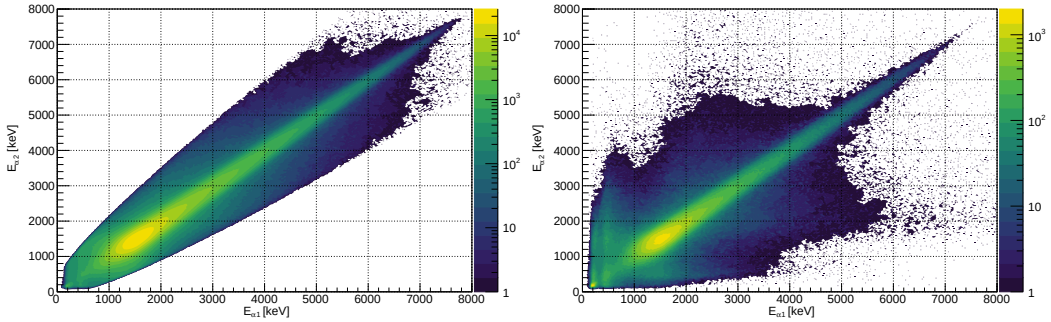

(c) A momentum cut. The total momentum of the particles must be less than 40 MeV/c

(d) A β-multiplicity cut. There must exist at least one β-particle and two α-particles in the event.

Figure 4.1: A collection of the different effects the cuts impose on the energy of the α-particles. On all the above figures, the energy of the first α-particle ($E_{\alpha 1}$) is plotted against the energy of the second α-particle ($E_{\alpha 2}$). The intensity scale is in logarithmic, to get a better view of all the different particle configurations.

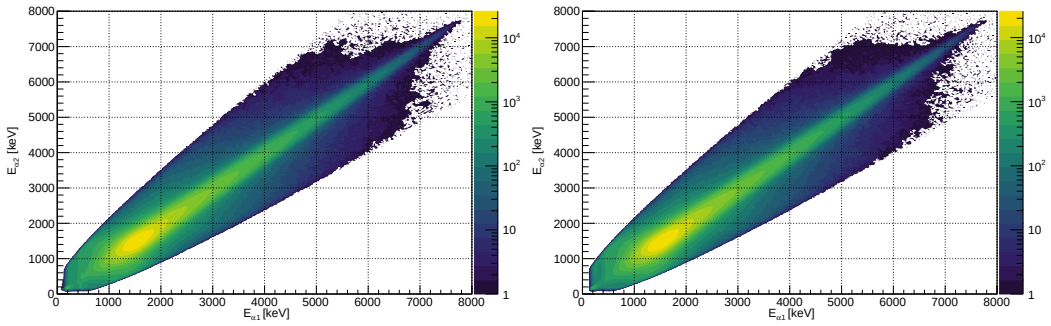

(a) Only moment **(b)** Ang and moment

Figure 4.2: A comparison of the momentum cut with and without the angular cut.

4.1.1 The effect of the angular cut

By imposing the angular cut, we get the first real reduction in data. If the angle between the two α-particles are less than $\cos(\theta) = -0.95 \approx 160°$, we sort away a good part of the β-α pairs, as seen on fig. 4.1b. But there are still a good portion of wrong pairs left, and we move on to impose a cut on the momentum of the particles.

4.1.2 The effect of the momentum cut

Again the aim is to sort the data, so that we can identify the particles. On fig. 4.1c the total momentum of the two particles has been limited to a maximum of 40 MeV/c. This cut sorts away all of the vertical and horizontal lines from a β-αpair. With this drastic cut, it looks like there is no use for the angular cut, which might be true. On figure 4.2 we can see the comparison of the effect of the momentum cut, with and without an angular cut. There does not seem to be a very large difference. Since momentum already takes the direction of the particles into account, as well as their energies, the angular cut will seem a bit redundant. However, we keep the angular cut on the data, as it will not take away any "good" measurements, but only some noise that slips through the multiplicity cut. Looking at fig. 4.4, we see the blue line as the momentum cut and the magenta line as the momentum and angular cut.

The two histograms lie very close to each other, except in the low energy ranger. Here we see a slight reduction in the magenta line, indicating that the pure angular cut will sort some β-particles from the data. It is therefor a justified cut to still impose on the data.

4.1.3 The effect of the multiplicity cut

The multiplicity of the β-particles should not interfere so much with the α-particles, but looking at fig. 4.1d, we see a drastic change in the pairs with energies far from each other. This is due to a general reduction in data. With the requirement that there must be one β-particle present in the event *and* that it must have hit either Det2 or DetD, we are left with a lot fewer measurements, which in turn gives a lower probability of noisy pairs.

4.1.4 The combined effect of all the cuts

By combining all of the cuts we are satisfied with the sorting of particles. On fig. 4.3 we see the effect of all the cuts. There is a very prominent line of particles with roughly the same energy. The line is thinner at higher energies, and widens as it goes towards lower energies. The reason for the widening, is the recoil energy from the β-decay. If the α-particles have low energy, they are more susceptible to other forces around it, and will lose a larger portion of their energy to the β-particle recoil.

On fig. 4.4 all the cuts are shown as individually, highlighting the effect that each cut provides. Here it is worth noting that not all β-particles have been successfully removed from the data. A slight peak at low energies still remain for the black line in the figure. This is also clear on fig. 4.3, where the there is a high intensity at the $\approx 200\,\text{keV}$ energy range.
An interesting effect that can be seen on the data, is the importance of the momentum cut. Looking the red and green line, we see a soft reduction in counts, different from the more rapid fall around 7 MeV. This is because there can be events where a particle will hit the detector, triggering it to measure, and before it turns completely off for detecting, another particle

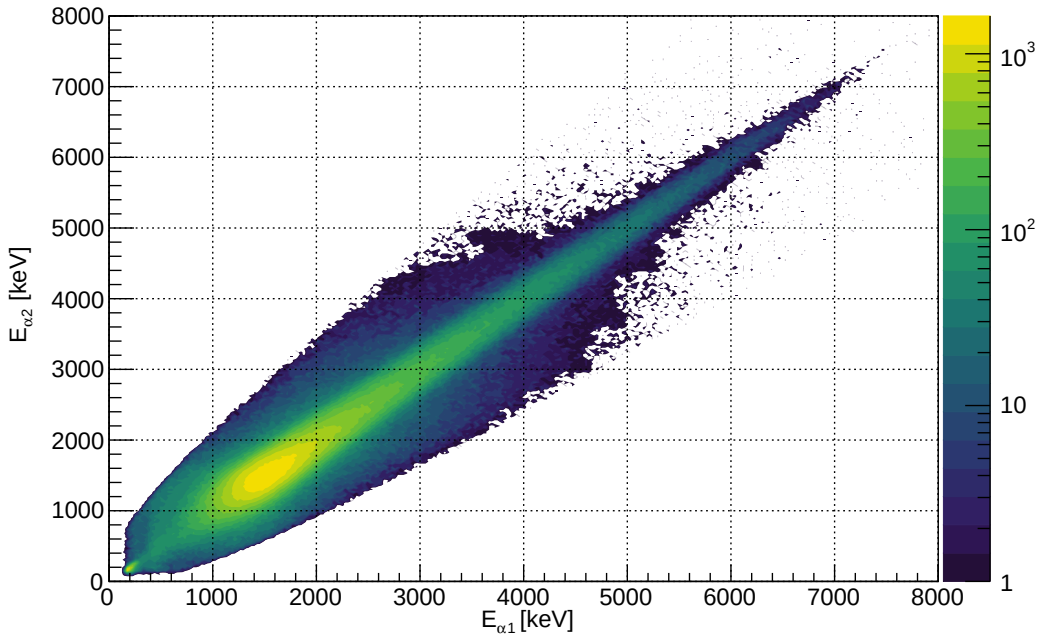

Figure 4.3: The energy of the first α-particle plotted against the energy of the second α-particle. All of the data reduction cuts are used here.

hits, and some of the the energies from both particles are measured as one particle.

So the momentum cut will also cut bad detection events away from the data in the high energy regime.

So far we have only considered that the α-particles are sorted correctly. But there is still a question for weather the β-particles will be clouded by wrong identifications. On fig. 4.5 we see the energy deposited in the two detectors that are capable of measuring β-particles, and the pad behind Det2. The energy from the pad and DetD, shows one peak around 400 keV and 300 keV, respectively. Det2 shows two peaks, one close to 400 keV, and one close to 800 keV. This is rather interesting, as we do not expect β-particles to deposit two different energies. Both detectors and the pad where 1000 μm thick, so we expect that the energy deposited would be roughly the same. The stopping power of silicon predicts an electron will deposit around 300 keV - 500 keV in 1000 μm silicon [9], depending on the actual energy of the β-particle. So the

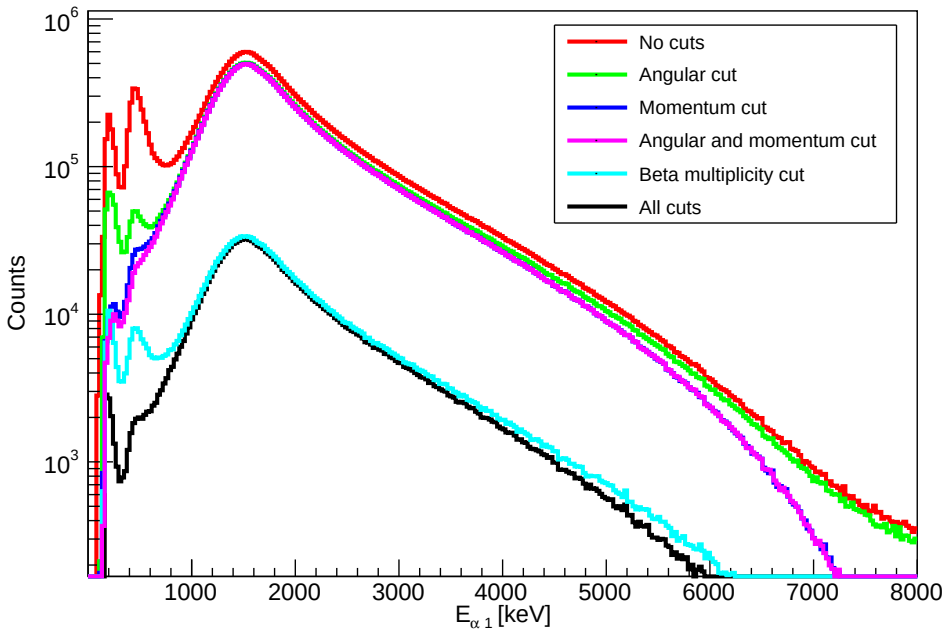

Figure 4.4: A comparison of all the cuts, with the energy of one α-particle shown.

first peak of the blue line is most likely the "real" β-energy. An explanation as to why we see the secondary peak, is could be that this detector was part of the trigger system, that detects when a particle has been hit anywhere in the setup. There is a lower bound on what energies that can trigger the system, and it is placed at 500 keV. So this peak most likely stems from false SOMETHING?.

4.2 The excitation energy of ^{8}Be

With the α-particles sorted correctly, we can start to look at the excitation energy of ^{8}Be. As mentioned in section 1.2.1 the β-decay of ^{8}Li will populate a broad exited state of ^{8}Be. This will give a more wide peak than we normally see in α-decays. On fig. 4.7 the energy sum of the α-particles has been plotted as the blue line. The peak lies closely to the mean energy of the exited state of 3.03 MeV, and then has a long tail all the way up to the around 16 MeV.

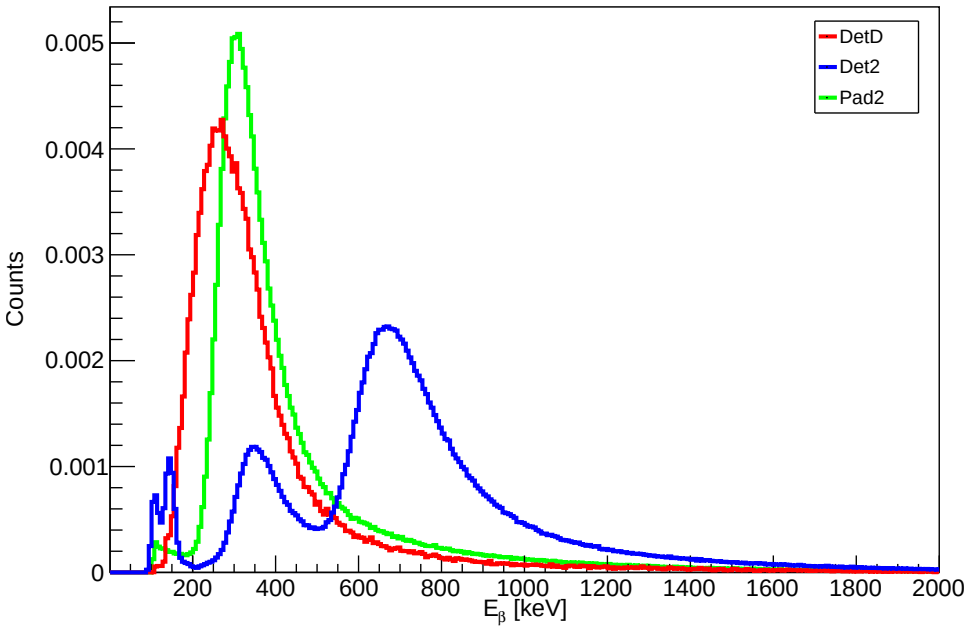

Figure 4.5: Energy deposited by β-particles in Det2 (blue), DetD (red) and Pad2 (green). PadD has been omitted, due to an error in the pad.

At the low end of the spectra, there is a small peak just before the beginning of the main peak. This is the reminiscence of low energy β-β pairs that have not been sorted in the data. We will not worry too much about this, as the interesting properties of the spectra lies at higher energies than the main peak.

The green line is a fit made to another experiment by Bhattacharya [10]. The fitted green line has been multiplied by 70 as to better compare the two plots. The plots differ a lot in the low energy range, as the β-particle contribution is rather prominent. But around the peak and at higher energy, the fit and our data follows nicely. At the very end, they differ again, as there seem to be some noise in our data, since the counts are too low to be considered otherwise.

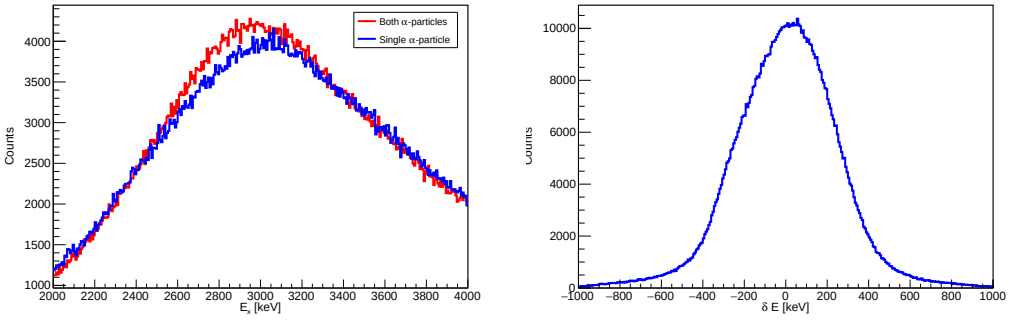

(a) Difference between twice the energy of one α-particle and the sum of two α-particles. The red line indicates the sum of both α-particles in coincidence. The blue line shows the double energy of a single α-particle.

(b) A plot of the difference in energy in the range 2 MeV to 4 MeV. The recoil of the leptons will have a notable difference in energies in this range.

Figure 4.6

4.2.1 Lepton recoil

E. K. Warburton [11] argues that the lepton recoil will be significantly small, and can be neglected, when observing the exitation spectra of ^{8}Be. This means that measuring one α-particle and multiplying the energy with 2, will be just as good a measurement as measuring both, and adding their energies. As Bhattacharya finds [12], it cannot be neglected, and as we have shown in fig. 4.6a and fig. 4.6b, the leptons will have a noticeable impact on the excitation of ^{8}Be, as it seems that the red line peaks at lower energies than the blue. The fit on fig. 4.5 from [10] also takes this effect into account.

4.3 Angular efficiency of the setup

Since the detectors are unable to cover the entire solid angle, there will always be some mutual angles that are more likely to be measured. If we only look at one detector, a very large number of angles are not covered, but small mutual angles such as $\theta \approx 0$, are very easy to measure, as it is just a measurement of two particles in the same pixel. This effect becomes apparent on

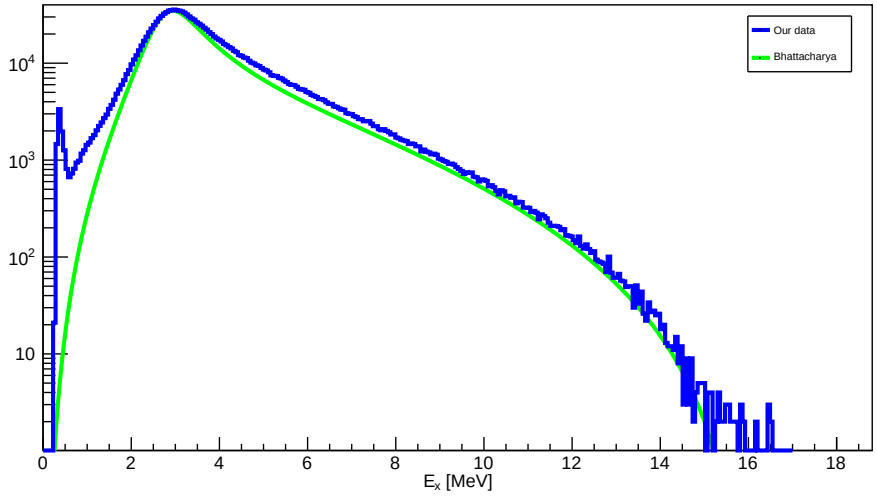

Figure 4.7: A comparison between the spectra of the excited state in ^{8}Be from this experiment(blue), and a fit found by Bhattacharya [10] (green).

fig. 4.8, where the angular efficiency is shown for Det2. For a single detector, there cannot be angles of $\theta = 90$ and higher, as the detector is flat. In this detector, the lowest angle found was $\theta = 77°$.

In this setup however, we have a cube of square detectors, who's normal vectors are all pointing in towards target at the center. This gives a much larger coverage of all mutual angles. The placement of the detectors gives that angles around $\theta \approx 90°$ are also very favored. This makes sense, almost no matter what pixel was hit, there is a corresponding pixel 90° to both sides. In the same way, will there always be a corresponding pixel $\approx 180°$ from each pixels. This effect can be seen on fig. 4.9.
This histogram was created using the spacial coordinates of each pixel in the setup. A list of all pixel position was gathered. The mutual angle between every pixel was found, that is $(16 \cdot 16 \cdot 6)^2 = 2{,}359{,}296$ possible angles in the setup.
There is still a geometric effect that is not accounted for in the above analysis. We need to consider that not all pixels in the detector has the same effective area. The pixel furthest out in a detector will have a effective area smaller

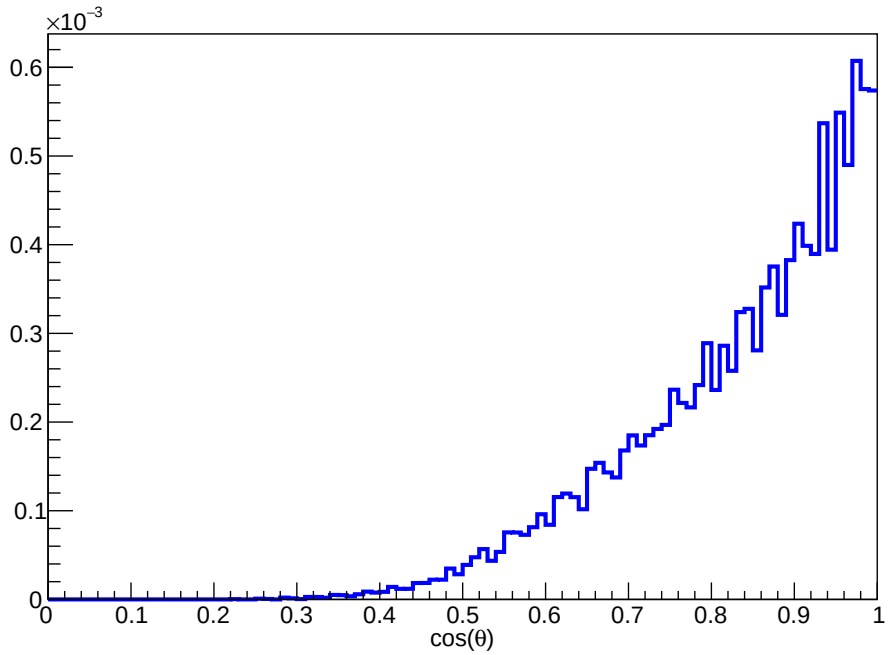

Figure 4.8: The angular efficiency of a single detector (Det2). For one flat detector, there can never be angles of 90° and higher. An efficiency has been multiplied to the histogram, which is why the y-axis is a bit arbitrary.

than the area of a pixel in the center. This effect can be seen on fig. 4.10a. Here we see that there is a much higher count of particles hitting the center of the detector, and fewer hitting the edges. A white line crossing through the middle is a defect strip, which did not measure anything. Sadly, some of the detectors had defect strips, which skews the effective angle and the measured.

To account for the geometric effects of the detectors, each pixel will be associated with a corresponding area-efficiency (Eff_A). This is calculated as

$$\text{Eff}_A = \frac{A\cos(\theta)}{4\pi r^2}, \tag{4.1}$$

where r is the distance to the pixel, A is the area of the pixel and θ is the angle between the hit direction and the normal vector of the detector as shown on fig. 4.11. As the angle becomes greater, the effective area of the

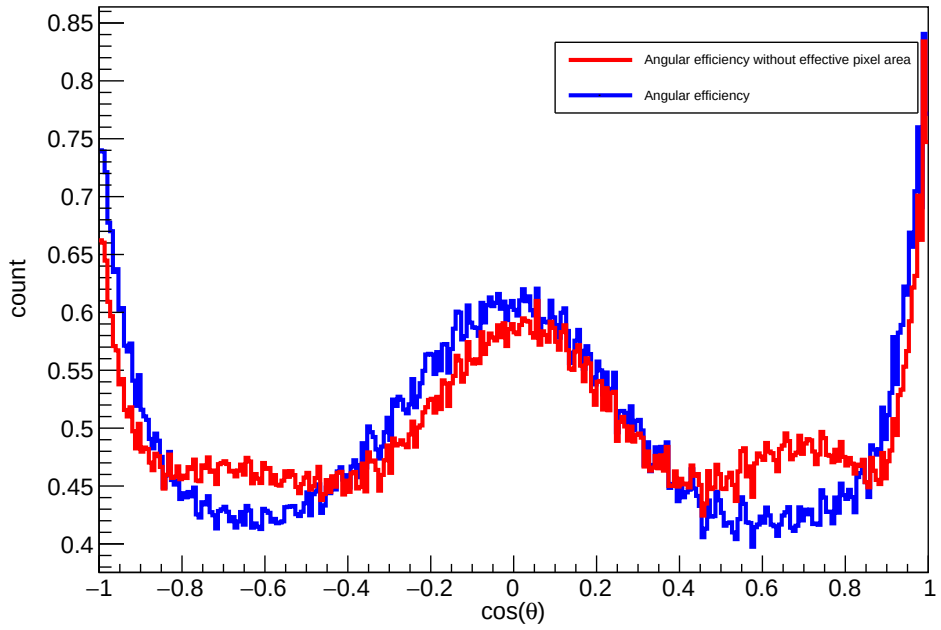

Figure 4.9: Two normalized histograms of the angular efficiency of the entire setup. The red histogram does not account for the effective area of a pixel. The blue is the true angular efficiency.

pixel decreases. The area of all pixel is the same for all detectors, so the constants A and 4π can be ignored when comparing the efficiency.

On fig. 4.9 two histograms can be seen. The red line represents the angular efficiency of the setup, without accounting for the relative area of the pixels, while the blue line is a weighted histogram for the same angles, with each pixels relative area accounted for.

The form of the two histograms are quite similar around 1, 0 and -1 but in between there is a rather prominent difference. Therefore it is important that the effective area of the pixel is accounted for, when we in section 4.4 will look at the angular correlations of the β-particle in the setup.

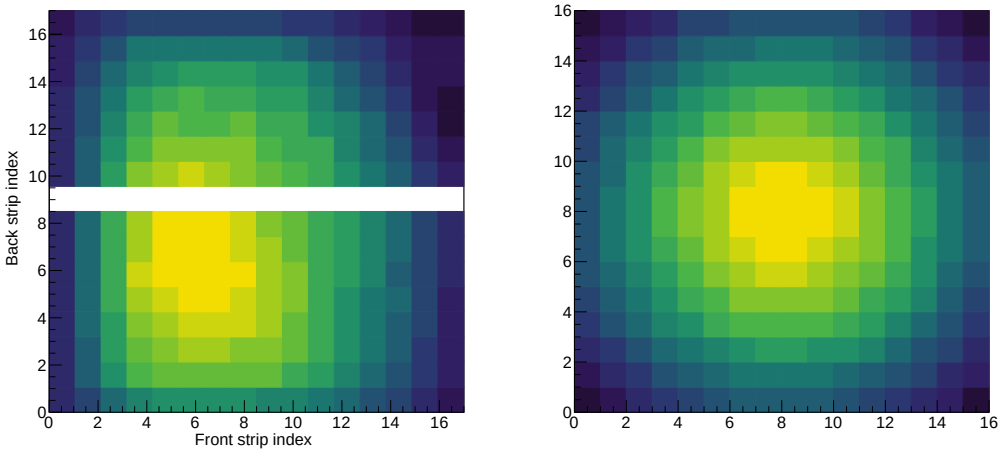

(a) A plot over the number of hits in each strip for Det2. The white line in the middle is a defect strip, that did not measure anything.

(b) A theoretical intensity Det2.

Figure 4.10

4.4 Angular correlations of α-particles and β-particles

From what we know in [2] the β-particles must have an isotropic distribution to the α-particles. This is done by first finding the angle between the first α-particle α_1 and the β-particle, and create a histogram of this. Then the angle between the second α-particle α_2 and the same β-particle is measured, and a histogram is created. The two histograms are then added, to get the full picture of the mutual angles of the particles. This can be seen on fig. 4.12 as the green line.

The blue line in this figure is the angular efficiency for the specific case, where the α-particles can hit in any given detector, but the β-particles can only hit in the two specific detectors Det2 and DetD. The two histograms has both been normalized, for a better comparison. By dividing the two histograms with each other, we get a better comparison. If they where to be close to equal, we would see a flat curve. But what we see on fig. 4.13 is not very flat.

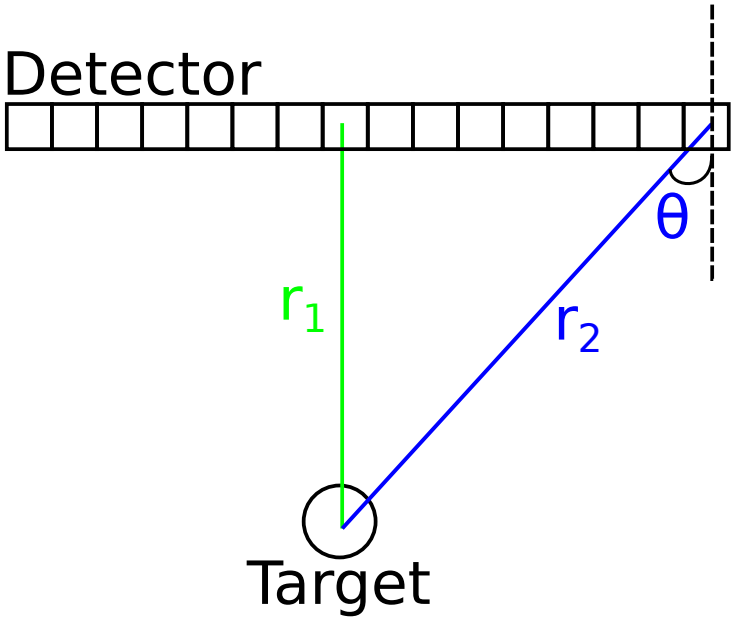

Figure 4.11: A illustration of two hits in different pixels. The blue hit will see a smaller effective area of the pixel by a factor determined by eq. (4.1), as the projection of the blue line onto the dashed line decreases as θ increases.

There are small fluctuations in the line, which stems from the inaccuracy of calculated angular efficiency. But the main shape of the curve is at most time not around $y = 1$.

There are two different explanations as to why this might be. The first explanation is that the beam did not hit the target in the center. The calculated efficiency assumes that the beam hits precisely in the middle, but in any setup, there can be a few millimeters of errors.

By finding the angular efficiency of the setup, with different values for the center and comparing this to the measured angles, we have found a slight correction for the center of the beam. This can be seen on fig. 4.14a, where the beam has been moved to the coordinates $(-3, -3, 0)$, as opposed to the previous of $(0, 0, 0)$. The division fo the two histograms on fig. 4.14b shows a more stable line from $\cos(\theta) = -0.4$ to $\cos(\theta) = 0.4$, but the edges are still not very alike. Looking at $\cos(\theta) = 1$, we see a rapid fall, which indicates that we have measured a lot fewer parallel β and α-particles than the setup is designed to handle. This can be due to the fact that some of the strips

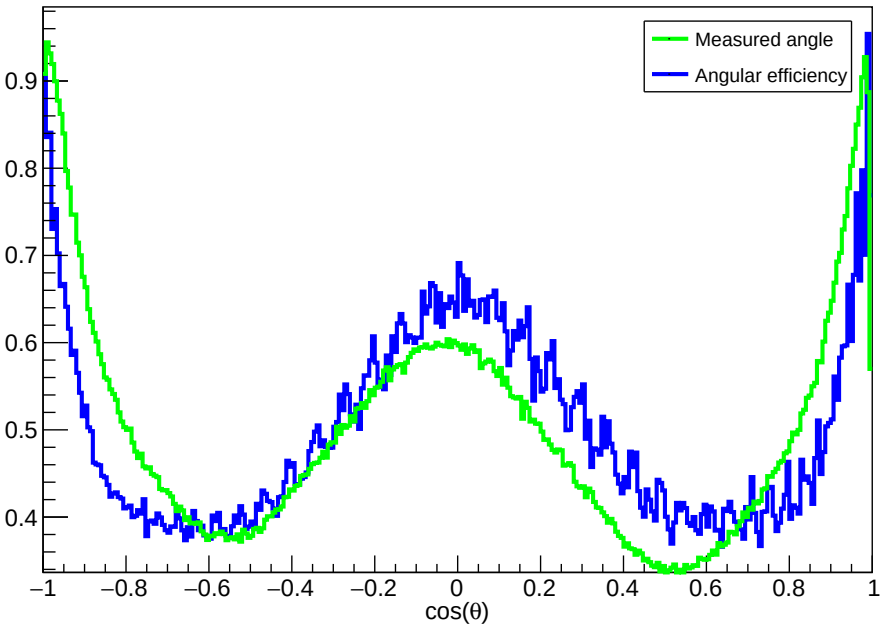

Figure 4.12: The measured β-α angular correlation is shown as the green line. The blue line shows the angular efficiency of the setup. Both histograms has been normalized, for a better comparison.

where defect. The calculated angular efficiency does not know which strips where defect, and and will therefore have a lot higher efficiency for parallel particles. The defect strips will therefore also play a role in the grand scheme, and is a possible explanation as to why there is a difference in the calculated and the measured data.

Another effect that will sway the data, is the target holder. This device will provide a shadow over the top and bottom detector, and since one of the β-detectors are the bottom one, it will skew the data in a unforeseeable way.

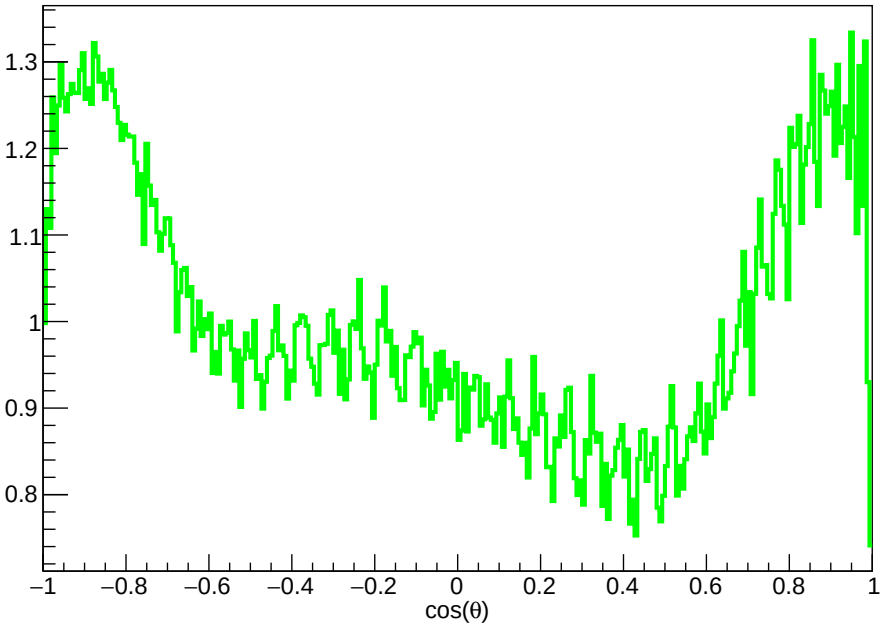

Figure 4.13: Data divided by the angular efficiency.

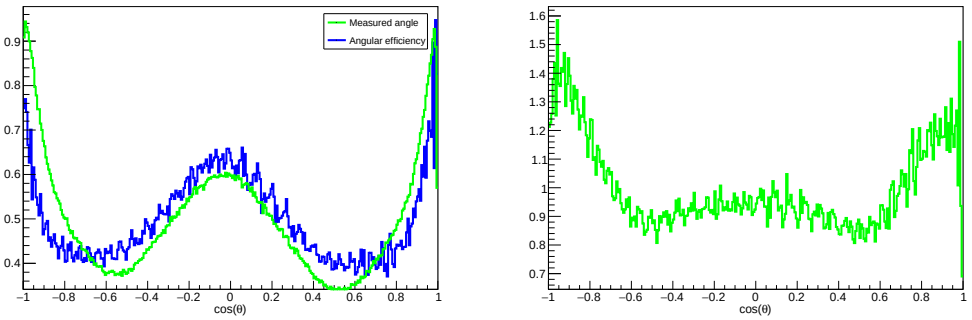

(a) The angular efficiency and the data, with a correction for the center of the beam.

(b) Measured β-α-particle angular distribution divided by the calculated angular efficiency of the setup, with a correction for position of the beam.

Figure 4.14

5 Conclusion

With coincidence measurements of β-delayed α-αbreakup of ^{8}Li, we have successfully measured the excitation spectrum of ^{8}Be. This spectrum has been compared to previous more precise measurements, and a nice consensus between the shape of the two measurements are shown.

The primary goal of the experiment was to measure the β-α angular correlations in the decay of ^{8}Li, since it is previously shown that this would be isotropic. Two decays was measured using this setup, ^{8}Li and ^{12}B, which involves a triple α-decay, and a β-decay. The setup was designed to measure α-particles position and energy with high resolution, as well as detecting β-particles position to equal resolution.
By comparing the excitation spectra of ^{8}Be, to previous measurements, we have shown that the setup has a satisfied energy resolution for α-particles. This has been further enhanced as it is shown that a good coincidence sorting will give a more precise α energy resolution.
When it comes to the β-α angular correlation, we have shown that there are some inconsistencies in the setup, that causes the angular analysis to more complex than first assumed. There is a good indication of the beam not hitting the exact center of the target, but there is also evidence of some detectors not being placed in a perfect cube around the target.
The target holder also casts a shadow on two of the detectors, which can further skew the measured angles away from the expected.

Bibliography

[1] Igisol. https://www.jyu.fi/science/en/physics/research/infrastructures/accelerator-laboratory/nuclear-physics-facilities/the-exotic-nuclei-and-beams.

[2] R. E. Tribble and G. T. Garvey. Induced weak currents and $\beta^{\pm} - \alpha$ angular correlations in $a = 8$. *Phys. Rev. C*, 12:967–983, Sep 1975.

[3] Andreas Gad. An experimental study of ^{8}B beta decay. Master Thesis. Aarhus University, Department of Physics and Astronomy, 2018.

[4] D.R. Tilley, J.H. Kelley, J.L. Godwin, D.J. Millener, J.E. Purcell, C.G. Sheu, and H.R. Weller. Energy levels of light nuclei a=8,9,10. *Nuclear Physics A*, 745(3):155–362, 2004.

[5] CERN. ROOT. https://root.cern/. 2021.

[6] M. Munch, J. Halkjær, and O. S. Kirsebom. Ausalib - aarhus subatomic library. https://git.kern.phys.au.dk/ausa/ausalib/wikis/home, 2017.

[7] ucesb. fy.chalmers.se/~f96hajo/ucesb/. Accessed June 10, 2021.

[8] James F. Ziegler, M.D. Ziegler, and J.P. Biersack. Srim – the stopping and range of ions in matter (2010). *Nuclear Instruments and Methods in Physics Research Section B: Beam Interactions with Materials and Atoms*, 268(11):1818–1823, 2010. 19th International Conference on Ion Beam Analysis.

[9] A. Kramida, Yu. Ralchenko, J. Reader, and and NIST ASD Team. NIST Atomic Spectra Database (ver. 5.8), [Online]. Available: https://physics.nist.gov/asd [2017, April 9]. National Institute of Standards and Technology, Gaithersburg, MD., 2020.

[10] M. Bhattacharya, E. G. Adelberger, and H. E. Swanson. Precise study of the final-state continua in ^{8}Li and ^{8}B decays. *Phys. Rev. C*, 73:055802, May 2006.

[11] E. K. Warburton. R-matrix analysis of the $\beta^{\mp}$-delayed alpha spectra from the decay of ^{8}Li and ^{8}B. *Phys. Rev. C*, 33:303–313, Jan 1986.

[12] M. Bhattacharya and E. G. Adelberger. Reanalysis of alpha + alpha scattering and the beta delayed alpha spectra from Li-8 and B-8 decays. *Phys. Rev. C*, 65:055502, 2002.